Multiscale Functional and Molecular Photoacoustic Tomography

Ultrasonic Imaging
2016, Vol. 38(1) 44–62

DOI: 10.1177/0161734615584312
ultrasonicimaging.sagepub.com

Junjie Yao[1], Jun Xia[1,2], and Lihong V. Wang[1]

Abstract

Photoacoustic tomography (PAT) combines rich optical absorption contrast with the high spatial resolution of ultrasound at depths in tissue. The high scalability of PAT has enabled anatomical imaging of biological structures ranging from organelles to organs. The inherent functional and molecular imaging capabilities of PAT have further allowed it to measure important physiological parameters and track critical cellular activities. Integration of PAT with other imaging technologies provides complementary capabilities and can potentially accelerate the clinical translation of PAT.

Keywords

photoacoustic tomography, photoacoustic microscopy, photoacoustic computed tomography, multiscale imaging, functional imaging, molecular imaging

Introduction

Photoacoustic (PA, also termed optoacoustic) tomography (PAT) is a hybrid imaging modality that acoustically detects the optical absorption contrast of biological tissue.[1-4] In PAT, the object is usually irradiated by a short-pulsed laser beam. Some of the incident photons are absorbed by biomolecules (e.g., hemoglobin, water, lipids, and melanin), and their energy is partially or completely converted into heat. The heat-induced pressure propagates in tissue as wideband ultrasound waves that are detected outside the tissue by an ultrasonic transducer or transducer array to form an image that maps the original optical energy deposition in the tissue.[5]

PAT seamlessly combines the rich optical absorption contrast of biological tissue with the high acoustic resolution at depths. In the optical excitation phase, a given percentage change in the optical absorption coefficient of the tissue yields the same percentage change in the linear PA signal amplitude; hence, PAT has 100% sensitivity to optical absorption contrast. In the acoustic detection phase, the ultrasound waves undergo only weak scattering in tissue, which enables high-resolution PA imaging at depths beyond the optical diffusion limit (~1 mm in tissue).[6]

[1]Optical Imaging Laboratory, Department of Biomedical Engineering, Washington University in St. Louis, MO, USA
[2]Department of Biomedical Engineering, University at Buffalo, The State University of New York, Buffalo, NY, USA

Corresponding Author:
Lihong V. Wang, Optical Imaging Laboratory, Department of Biomedical Engineering, Washington University in St. Louis, MO 63130 USA.
Email: lhwang@wustl.edu

Benefiting from fast advances in laser and ultrasound technologies, PAT has developed remarkably since the early 2000s.[7-9] Almost all the key performance aspects of PAT, including spatial resolution, penetration depth, imaging speed, and detection sensitivity, have been continuously improved through collaborative efforts involving engineering, mathematics, materials science, chemistry, and biomedicine. Building on these technical advances, PAT has become increasingly popular in preclinical studies, especially in studying tumor angiogenesis, cancer hypoxia, brain functions, tissue remodeling, and drug delivery.[1,2] Most encouragingly, PAT has started to be used in clinical practice, for procedures such as breast cancer screening,[10-12] sentinel lymph node mapping,[13-18] melanoma staging,[19-24] and endoscopic examination.[25,26] All of these preclinical and clinical applications of PAT are important maturing steps toward human health care.

In light of the deep connections between PAT and ultrasound imaging,[5,27] this concise review aims to introduce PAT technologies to the general ultrasound community, highlighting its inherent functional and molecular imaging capabilities. Representative PAT applications in both fundamental studies and clinical practice will be reviewed. Integration of PAT with other imaging modalities will also be discussed, and finally, potential PAT technical breakthroughs will be envisioned.

Multiscale PAT: Seeing Clearly at Depths

Photon propagation in soft tissue can be loosely classified into four regimes, which are approximately related to the penetration depths of representative optical imaging modalities (Figure 1a).[5,28] Conventional planar optical microscopy works within the aberration limit (~~100 μm, ballistic regime), where photons have undergone no scattering.[5] Modern optical imaging modalities, such as confocal microscopy, two-photon microscopy, and optical coherence tomography, are limited by diffusion to ~1 mm in soft tissue (quasi-ballistic regime), where scattered photons still retain strong memory of original propagation direction.[4] Diffuse optical tomography (DOT) and PAT are able to provide penetration into the quasi-diffusive and diffusive regimes where photons have almost completely lost their memory of the original propagation direction.[5,32,33] However, DOT and PAT are still limited by dissipation to less than 10 cm in soft tissue, where the optical fluence (J/m^2) is significantly attenuated due to both absorption and scattering. Finally, when the optical scattering is largely corrected for by using wavefront engineering technologies, it is believed to be possible to conquer the dissipation limit and approach the absorption limit (~1 m) for whole-body penetration in humans.[34,35] For brevity, the following use of "diffusive" and "ballistic" in this review also refers to "quasi-diffusive" and "quasi-ballistic," respectively.

In contrast, ultrasound attenuation in soft tissue is dominated by absorption instead of scattering.[29,36] For example, at 5 MHz, the ultrasound scattering coefficient of the human skin is 0.014 cm^{-1}, whereas the ultrasound attenuation coefficient is 0.38 cm^{-1}. The ultrasound attenuation coefficient is approximately proportional to the ultrasound frequency over a wide frequency range.[29-31] In fact, a good rule of thumb is that the ultrasound attenuation coefficient for a variety of soft tissues is 0.5 to 1.0 dB/cm/MHz.[29] Such frequency-dependent attenuation in ultrasound imaging results in the trade-off between its spatial resolution and penetration depth. Figure 1b shows the approximate ultrasound penetration depths at typical frequencies and the corresponding biomedical applications.

Since PAT utilizes optical excitation and acoustic detection, its resolution can be either optically or acoustically determined, depending on the targeted penetration depth. Classified by how its resolution is determined, PAT has two major implementations[1]: acoustic-resolution PAT with an imaging depth beyond the optical diffusion limit and optical-resolution PAT with an imaging depth less than the optical diffusion limit. Readers are referred to recent review articles for comprehensive details about different PAT implementations.[3,37-39]

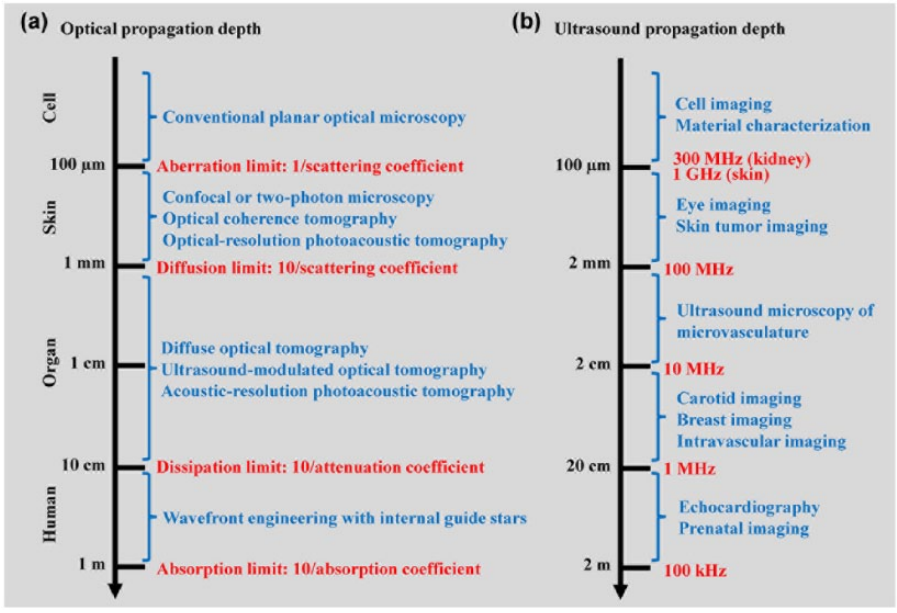

Figure 1. Photon and ultrasound propagation regimes in soft tissue. (a) Photon propagation regimes in soft tissue, which are approximately related to the penetration depths of representative optical imaging modalities.[5,28] The four regimes are divided at photon propagation depths of 0.1 mm, 1 mm, 10 cm and 1 m, with typical optical absorption coefficient of 0.1 cm^{-1}, optical scattering coefficient of 100 cm^{-1}, and anisotropy of 0.9. The classification holds in optical scattering dominant media. (b) Ultrasound propagation regimes at typical ultrasound frequencies in soft tissue, with corresponding biomedical applications.[29] The ultrasound attenuation coefficient is approximately proportional to the ultrasound frequency up to at least 300 MHz for skin[30] and 100 MHz for kidney.[31] Here, the −10 dB propagation depth at the frequency up to 100 MHz is estimated with an ultrasound attenuation coefficient of 0.5 dB/cm/MHz. The propagation depths at 300 MHz for kidney and 1 GHz for skin are extrapolated based on the literature data,[30,31] taking into account the ultrasound attenuation by water.

Acoustic-Resolution PAT

Acoustic-resolution PAT targets deep tissue imaging with acoustically determined resolutions in all dimensions. Acoustic-resolution PAT can be implemented by raster-scanning weakly focused optical illumination and a spherically focused ultrasonic transducer, a technology typically referred to as acoustic-resolution photoacoustic microscopy (AR-PAM). Acoustic-resolution PAT can also be implemented by using wide-field optical illumination and parallel acoustic detection with an ultrasonic transducer array, a technology typically referred to as photoacoustic computed tomography (PACT). In acoustic-resolution PAT, both the spatial resolution and imaging depth are highly scalable with the ultrasound frequency. PAT operating with lower ultrasound frequency can penetrate deeper with relaxed resolution.

As a rule of thumb, different acoustic-resolution PAT embodiments have generally achieved a depth-to-resolution ratio (DRR) of ~200.[1] For example, by using a 50 MHz focused ultrasonic transducer, the first AR-PAM achieved a lateral resolution of ~45 μm, an axial resolution of ~15 μm, and an imaging depth of ~3 mm in tissue.[8,40] Such an imaging depth is sufficient for melanoma staging[40] and pain treatment evaluation[41] in the human skin. By using a similar design but

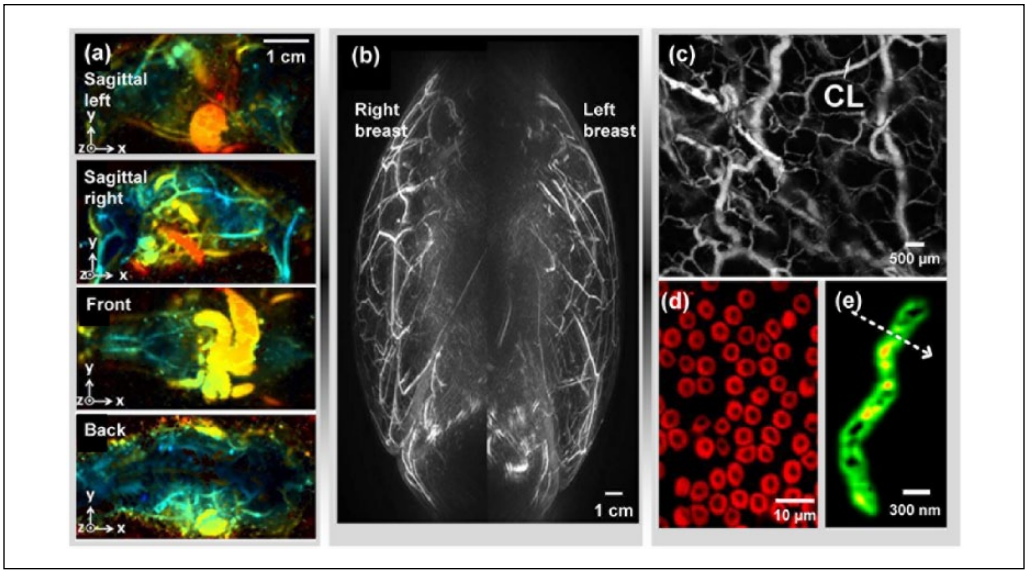

Figure 2. Multiscale PAT. (a) Whole-body PAT of a mouse *in vivo*.[43] Acquired at 1064 nm, the MAP images were extracted from sagittal, front, and back views. The depths are color encoded from blue (shallow) to red (deep). (b) Medial-lateral MAP image of breasts of a healthy volunteer.[12] A semispherical transducer array was used with rotational scanning. (c) OR-PAM of mouse ear vasculature, where single capillaries (CL) can be clearly resolved.[44] (d) Subwavelength OR-PAM of single red blood cells.[45] A lateral resolution of ~220 nm was achieved. (e) Photoacoustic nanoscopy of a mitochondrion in a fibroblast cell.[46] A lateral resolution of ~80 nm was achieved by using the optical absorption saturation effect. Images were adapted with permission from references. PAT = photoacoustic tomography; MAP = maximum amplitude projection; OR-PAM = optical-resolution photoacoustic microscopy.[12,43-46]

with a 5 MHz transducer, photoacoustic macroscopy (PAMac) increased the imaging depth to ~38 mm, with a relaxed lateral resolution of ~500 μm and axial resolution of ~144 μm.[42,43] This imaging depth is sufficient for whole-body mouse imaging (Figure 2a)[43] and deep sentinel lymph node mapping.[13-18]

Acoustic-resolution PAT has proven powerful in deep tissue imaging, such as human breast cancer detection,[11-13,47-49] prostate adenocarcinoma imaging,[50,51] atherosclerotic plaque characterization,[26] ophthalmic imaging,[52] gastrointestinal (GI) tract imaging,[53] small animal whole-body imaging,[54-56] and thyroid imaging.[57] Of all the clinical translations of PAT, human breast imaging has progressed furthest. So far, several groups have reported PA breast imaging on a total of more than 100 patients.[37] To accommodate the shape of the uncompressed breast, Kruger and his colleagues used a semispherical transducer array with rotational scanning for dense spatial sampling (Figure 2b).[12] However, this configuration suffers from low imaging speed and may have difficulty in detecting deep tumors. Kitai and his colleagues used a 2D planar transducer array, where the breast was gently compressed from the side between a glass slide and the transducer array.[48] The side compression can reduce the effective breast thickness and thus help detect deeper tumors. However, the planar detection geometry suffers from limited view for accurate reconstruction. Alternatively, our laboratory has developed an integrated PAT and thermoacoustic tomography (TAT) system, where the breast is compressed from the front (the nipple side) to form a cylindrical shape.[58] The illumination is directed from the front, and the ultrasonic transducers scan around and along the cylindrical breast to obtain a full 3D data set. In this configuration, deep tumors close to the chest wall can potentially be imaged.

Optical-Resolution PAT

Although acoustically determined resolutions in acoustic-resolution PAT are adequate for many biomedical applications, it becomes challenging to improve the spatial resolutions to the cellular level by simply increasing the ultrasound frequency without severely compromising the penetration.[29,59,60] Different from ultrasound imaging, PAT can use fine optical focusing to provide optically defined lateral resolution within the optical diffusion limit, whereas the axial resolution is still derived from the time-resolved ultrasonic detection.

Optical-resolution PAT is traditionally referred to as optical-resolution photoacoustic microscopy (OR-PAM).[44,55,61-76] Limited only by optical diffraction, the lateral resolution of OR-PAM can easily reach the cellular and subcellular level and is scalable with the optical wavelength and the numerical aperture (NA) of the optical objective. The first OR-PAM, reported in 2008, achieved a lateral resolution of ~5 μm (objective NA: 0.1 in air) and an imaging depth of ~1 mm. Single capillaries in a mouse ear can be clearly resolved (Figure 2c).[44] The lateral resolution of OR-PAM was later improved to ~220 nm by using a water-immersion objective (objective NA: 1.23 in water), allowing single red blood cells to be clearly resolved (Figure 2d).[45] Furthermore, in recently developed optical-resolution PACT systems, the field of view is simultaneously excited by an array of diffraction-limited optical foci, and the resultant PA waves are detected by a linear- or ring-shape ultrasonic transducer array.[71,77,78] The parallel excitation and detection enable fast wide-field imaging, whereas the imaging depth is still restricted to ~1 mm.

Recently, OR-PAM has succeeded in suboptical-diffraction imaging, taking advantage of various nonlinear mechanisms such as two-photon absorption,[79-81] photobleaching,[82] absorption saturation,[83] and thermal relaxation.[83,84] Nonlinear OR-PAM has provided optically determined resolutions in all dimensions including the axial or depth direction. In particular, a subdiffraction lateral resolution of ~80 nm has been achieved by photoacoustic nanoscopy using the absorption saturation effect, enabling single mitochondria in fibroblast cells to be resolved (Figure 2e).[83] Meanwhile, an axial resolution on the level of submicrometers has been achieved, which is about two orders of magnitude finer than the acoustically determined axial resolution in traditional linear OR-PAM.[82,83]

Functional and Molecular PAT: Seeing More than Anatomy

Although functional ultrasound imaging is largely limited to Doppler ultrasound, and molecular ultrasound imaging mostly detects microbubbles in the vasculature,[27] PAT is inherently suited for diverse functional and molecular imaging, with a wealth of endogenous and exogenous contrasts.

Functional PAT

So far, PAT has measured a number of functional parameters at various length scales, including total hemoglobin concentration,[12,66,85-87] blood oxygenation,[86-93] temperature,[94-96] blood flow,[95,97-103] pH,[104-107] blood glucose level,[108] pulse-wave velocity,[109] and metabolic rate of oxygen (MRO_2).[22,110,111] Here we discuss several widely measured functional parameters, especially for cancer diagnosis and therapy.

Hemoglobin in red blood cells carries most of the oxygen needed by the body to power its functions.[112] Using hemoglobin as the endogenous contrast, PAT can quantify the total hemoglobin concentration (HbT) and oxygen saturation of hemoglobin (sO_2) with high sensitivity (Figures 3a-b).[114] For accurate measurement of absolute HbT and sO_2, it is necessary to correct for light attenuation by using empirical or model-based methods.[90-92,115-118] Recently, single-wavelength-based and dynamics-based PA methods have also been developed for absolute sO_2 measurement.[89,119] Notably, HbT

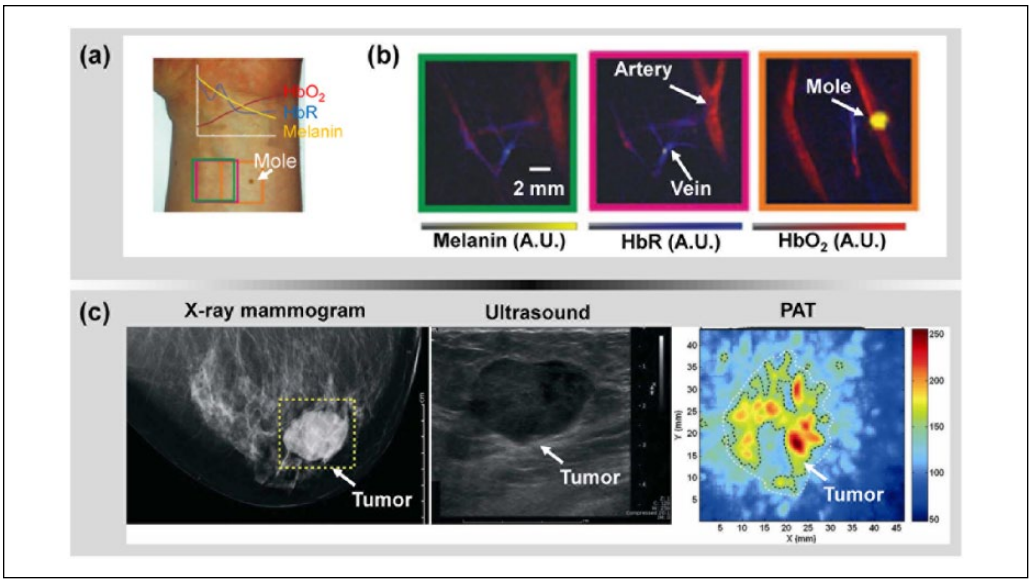

Figure 3. Functional PAT. (a) A photograph of a healthy volunteer's forearm, from which hand-held PACT images were taken.[113] The colored boxes correspond to the regions of interest imaged by PACT: HbR, deoxy-hemoglobin; HbO_2, oxy-hemoglobin. (b) Spectrally unmixed PA oxygenation images of the three boxed regions shown in (a). (c) PAT of an invasive ductal carcinoma in the right breast of a 57-year-old woman.[48] Left to right: X-ray mammogram (left), ultrasound image (middle), and PAT image (right). The higher PA signal strength in the PAT image was attributed to tumor angiogenesis. Images were adapted with permission from references. PAT = photoacoustic tomography; PACT = photoacoustic computed tomography; PA = photoacoustic.[48,113]

and sO_2 measurements are proven useful in cancer diagnosis and prognosis. For example, in PA breast cancer imaging, increased HbT in the tumor region is highly correlated with cancer angiogenesis (Figure 3c),[48] whereas decreased sO_2 in the tumor core typically indicates an adverse cancer progression.[120,121]

During thermotherapy, it is necessary to monitor the local temperature for safe deposition of heat and efficient destruction of abnormal cells. Using the temperature dependence of the Grueneisen parameter,[122-129] PAT can measure temperature changes from relative changes in PA amplitude alone.[94,130] A temperature detection sensitivity of 0.15°C was achieved with a temporal resolution of 2 s.[94] Furthermore, a recently published method can quantify the absolute temperature in deep tissue with AR-PAM and PACT, using the dual temperature dependences of the Grueneisen parameter and the speed of sound (SOS).[131,132] In addition to measuring temperature, the temperature dependence of PA signal can also be used to measure the blood flow speed in deep tissue,[95,133] enhance the spatial resolution of OR-PAM,[83] and ameliorate the limited-view problem in linear-array-based PACT.[133]

Blood flow ensures the transportation of oxygen, nutrients, and metabolic wastes throughout the body. PAT can measure blood flow by using either Doppler methods[98,100,102,103, 134-137] or feature-tracking methods.[95,99,101,138,139] Compared with ultrasound flowmetry, PA flowmetry has much higher detection sensitivity because of the excellent contrast between the blood vessels and the surrounding tissue. A flow detection sensitivity of 50 μm/s has been demonstrated by using a structured-illumination PA method.[137] In addition, thermal-tagging methods have measured flow speeds at 5 mm depth in tissue.[95,101,138,139] Consequently, by simultaneously measuring multiple

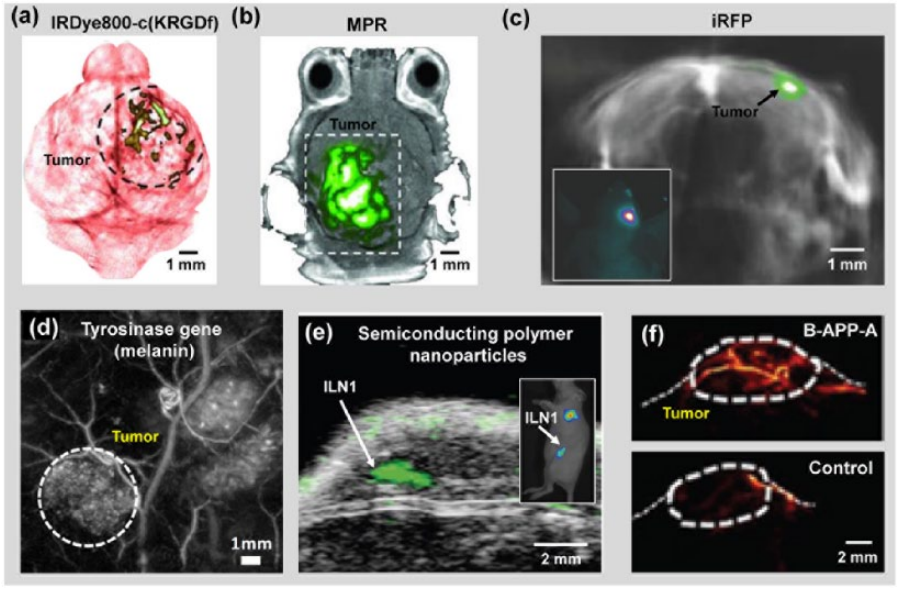

Figure 4. Molecular PAT. (a) PAT of a glioblastoma in a mouse brain enhanced by IRDye800-c(KRGDf), which targeted overexpressed integrin $\alpha_v\beta_3$ in tumor cells.[7] (b) PAT of a glioblastoma in a mouse brain enhanced by tri-modality MRI-PA-Raman (MPR) nanoparticles.[83] (c) PAT of an iRFP-expressing glioblastoma in a mouse brain, 25 days post implantation.[148] The spectrally unmixed signals from the tumor (shown in green) are superimposed on the signals from blood (shown in gray). iRFP = infrared fluorescent protein. Inset: epi-fluorescence image of the mouse brain showing the tumor location. (d) PAT of a subcutaneous tyrosinase-expressing tumor.[149] The tumor is marked by the dashed circle. (e) Ultrasound (shown in gray) and photoacoustic (shown in green) coregistered image of mouse lymph nodes following tail vein injection of semiconducting polymer nanoparticles (SPN).[150] ILN = inguinal lymph node. Inset: epi-fluorescence image of the mouse showing the ILN location. (f) PAT of the activatable B-APP-A in a human follicular thyroid cancer FTC133 in the mouse hind leg after tail vein injection of B-APP-A (top) and the control probe (bottom).[57] Images were adapted with permission from references. PAT = photoacoustic tomography; MRI = magnetic resonance imaging; PA = photoacoustic.[7,57,83,148-150]

parameters such as HbT, sO_2, and blood flow, PAT can quantify the MRO_2 of tissue, which can potentially be used for early cancer detection.[22,110,111]

Molecular PAT

In addition to functional imaging, by using targeted or untargeted contrast agents, PAT can track molecular processes in living organisms.[21,134,140-146] The choice of contrast agents for molecular PAT is much greater than for molecular ultrasound imaging, because all molecules have their own absorption wavelengths, hence they can be imaged by PAT.[38,39] In addition, many molecules can reach the extravascular space. So far, many contrast agents have been imaged in molecular PAT,[37,38,147] including organic dyes (Figure 4a), nanoparticles (Figure 4b), fluorescent proteins (Figure 4c), microbubbles, and reporter gene products (Figure 4d). These contrast agents, especially nanoparticles,[142] can be specifically engineered for different PA applications.

The detection sensitivity of molecular PAT is relevant to a number of factors, such as the absorption cross-section of the molecule, the sensitivity of the ultrasonic transducer, the imaging depth,

and the permitted light exposure.[151] Roughly, in molecular PAT, the reported noise-equivalent detectable concentration at ≥3 mm depth in tissue is on the level of millimolar for microbubbles, micromolar for organic dyes, nanomolar for proteins, and picomolar for nanoparticles.[47,152-157]

Molecular PAT has been proven reliable in early cancer imaging, circulating tumor cell (CTC) detection, glucose uptake monitoring, and sentinel lymph node mapping (Figure 3e).[155,158,159] For example, PAT has been successfully used for detecting pigmented circulating melanoma cells, due to their strong light absorption.[21,160,161] Recently, nonpigmented circulating breast cancer cells have also been detected *in vivo* by PAT, using targeted gold nanoparticles[162] or genetically encoded green fluorescent protein[163] as the contrast agent. Multispectral PA measurements can help unmix different molecules to enhance the detection of CTCs[143] and early-stage tumors.[148] Magnetically modulated PA detection can highlight the signals from magnetic nanoparticles targeted to tumor cells.[143] Activatable organic dyes and nanoparticles can also help detect cellular activities of interest, with improved sensitivity (Figure 3f).[57,160]

It is worth noting that multiwavelength illumination is often required in functional and molecular PA imaging. However, commercially available wavelength-tunable lasers (e.g., dye lasers, optical parametric oscillators, or Ti: sapphire lasers) cannot switch wavelengths at a high speed.[164] Several methods have been developed to achieve fast wavelength tuning. Dean-Ben and his colleagues customized a 50 Hz optical parametric oscillator that allowed wavelength change on a per-pulse basis for their hemi-spherical-array-based PACT.[113] Wang et al. have developed a digital-mirror-device-based wavelength multiplexing method for OR-PAM with a wideband dye laser.[116] A 2 kHz wavelength tuning speed has been achieved with a wavelength-tunable range of ~20 nm. In addition, two lasers with different wavelengths can serve as an alternative to wavelength tuning, with increased system cost.[165]

Integration of PAT with Other Imaging Modalities

A major challenge for quantitative PAT is the unknown local light fluence. This issue can potentially be addressed by integrating PAT with DOT, which measures the optical properties of the tissue. Multiple groups have reported various DOT-PAT systems for different applications.[97,166-168] Studies have shown that DOT allows better quantitative reconstruction in PAT.[166,167,169] However, the optical properties derived from DOT measurements typically possess much poorer spatial resolution than that of PAT. Iterating between PAT and DOT reconstructions may help resolve this issue.[167]

SOS heterogeneities also deteriorate PAT image quality. One remedy is to combine PAT with ultrasound tomography (UST). In UST-PAT systems, UST provides the SOS map of the tissue to improve the PAT reconstruction. Unlike the combination of PAT with DOT, which requires additional light sources and detectors, the addition of UST to PAT can be implemented with existing ultrasonic transducers as long as the ultrasonic transmission capability is enabled.[170] Alternatively, PAT can be integrated with commercial UST by adding a pulsed light source.[13] In addition to heterogeneous SOS, acoustic attenuation and aberration also deteriorate PAT image quality,[170-173] especially in human brain PAT, but their effects can be potentially investigated with UST-PAT as well.

In addition to correcting for optical and acoustic inhomogeneities, different PAT embodiments have also been integrated with other imaging modalities to provide complementary contrasts.[174] Deep-penetration imaging modalities, such as magnetic resonance imaging (MRI), X-ray computed tomography (CT), and positron emission tomography (PET), have been used in conjunction with PAT for studies involving multimodality contrast agents.[24,149,175] PAT has been integrated with confocal microscopy,[176,177] optical coherence tomography,[178-181] and ultrasound imaging,[13,18,26,53,55,182,183] sharing either the same optical components or ultrasonic transducer(s) (Figure 5a).[53] A recently

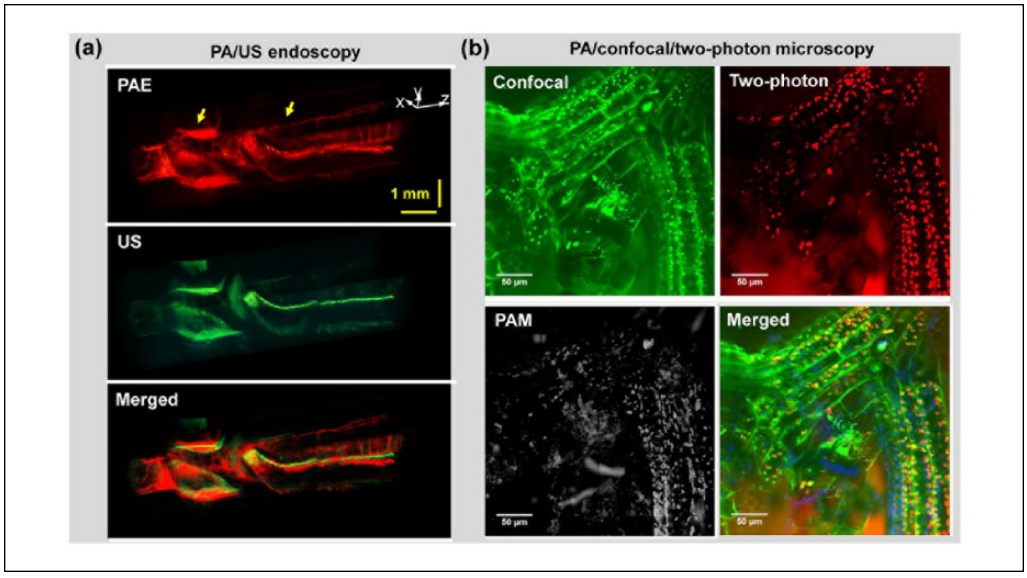

Figure 5. Integration of PAT with other imaging modalities. (a) Integrated PA/US endoscopy of the upper esophagus of a rabbit *in vivo*.[53] The PA and US imaging share the same ultrasound transducer and scanning system. (b) Integrated PA/confocal/two-photon microscopy of a moss leaf.[184] The three imaging modalities share the same optical paths and scanning system. Images were adapted with permission from references. PAT = photoacoustic tomography; PA = photoacoustic; US = ultrasound.[53,184]

developed tri-modality optical imaging system combines OR-PAM with a commercial confocal and two-photon microscopic system (Figure 5b).[184] The three imaging modalities can readily share the optical illumination path and scanning system.

Discussion

In conclusion, PAT is a unique imaging modality that complements other imaging techniques: rich optical absorption contrast provides inherent functional and molecular imaging capabilities, and acoustic detection allows high-resolution imaging at depths. Although we can cover only several representative studies in this concise review, they have clearly shown the scale and momentum of PAT development. Here, we will also discuss a few potential breakthroughs of PAT technologies.

One new frontier is PA-based optical wavefront engineering. The ability to focus light deep into tissue will have tremendous impacts on imaging and therapy. By using PA signals as the feedback, the wavefront of the excitation light can be optimized through iterative algorithms so that it can be confined to either an acoustically or optically determined region in the tissue.[185,186] The advantage of PA detection is its high resolution and deep penetration, although the slow optimization process remains to be a major challenge.

Miniaturizing the PA probe is essential for endoscopic and intravascular applications. Recently, several PA endoscopes have been developed with optical detection of the acoustic signals.[187-190] Since the detection sensitivity of these optical detectors (e.g., microring resonators and Fabry–Perot sensors) is not directly related to the detector size, the PA probe size can be significantly reduced. However, none of those optical detectors have been used for acoustic-resolution endoscopic imaging in deep tissue, due to the lack of acoustic focusing capability. Alternatively,

internal optical illumination through the body cavity can be combined with external acoustic detection,[191] avoiding the problem of acoustic detector size.

There is also great interest in hand-held PA probes for imaging surface regions such as the face, neck, and arm, which are difficult to access with traditional table-top PAT systems. Several hand-held PA probes have been developed for microvascular imaging of port-wine stains on the face,[192,193] blood oxygenation imaging of the jugular vein in the neck,[194] sentinel lymph node mapping in the breast,[195] and melanoma imaging on the skin.[196,197] For these hand-held PA probes, the imaging speed still needs to be improved to mitigate motion artifacts from both the patient and operator.

Although PAT is relatively inexpensive compared with MRI and PET, further reducing its cost can accelerate clinical translation. The most expensive components in PAT are typically the pulsed laser source and the ultrasonic transducer array. Several groups have explored inexpensive light sources.[181,198-202] For example, Li et al. have developed an OR-PAM system using a low-cost Blue-ray DVD pickup head with a 405 nm laser diode.[203] An inexpensive ultrasound detector is also of interest because the ultrasound receiving system becomes significantly more costly as the number of transducer elements increases. A PAT system based on low-cost acoustic delay lines for acoustic detection has been reported.[203,204] Nevertheless, the acoustic coupling efficiency and the number of the acoustic delay lines still need to be increased.

At last, with its nonionizing radiation, high-image quality, and functional and molecular imaging capabilities, PAT holds great promise for disease detection, staging, and treatment evaluation. Although many challenges remain, none of them are beyond reach. PA breast cancer screening is now most ready for clinical translation. PA endoscopic examination of the GI tract will provide functional information at unprecedented depths. PA melanoma detection at depths up to a few millimeters will significantly improve the cancer's staging accuracy. Finally, PA human brain imaging through intact scalp and skull, although technically challenging, is considered one of the most promising tools for functional brain studies, with breakthroughs expected soon.

Acknowledgment

The authors appreciate Prof. James Ballard's close reading of the manuscript.

Declaration of Conflicting Interests

The author(s) declared the following potential conflicts of interest with respect to the research, authorship, and/or publication of this article: L. V. Wang has a financial interest in Endra, Inc., and Microphotoacoustics, Inc., which, however, did not support this work.

Funding

The author(s) disclosed receipt of the following financial support for the research, authorship, and/or publication of this article: This work was sponsored in part by NIH Grants DP1 EB016986 (NIH Director's Pioneer Award), R01 CA186567 (NIH Director's Transformative Research Award), and U01 NS090579 (BRAIN Initiative).

References

1. Wang LV, Hu S. Photoacoustic tomography: in vivo imaging from organelles to organs. Science. 2012;335:1458-62.
2. Wang LV. Multiscale photoacoustic microscopy and computed tomography. Nat Photonics. 2009;3:503-9.
3. Beard P. Biomedical photoacoustic imaging. Interface Focus. 2011;1:602-31.
4. Ntziachristos V. Going deeper than microscopy: the optical imaging frontier in biology. Nat Methods. 2010;7:603-14.

5. Wang LV, Wu H-I. Biomedical Optics : Principles and Imaging. Hoboken, NJ: Wiley-Interscience; 2007.
6. Yao J, Wang LV. Photoacoustic tomography: fundamentals, advances and prospects. Contrast Media Mol Imaging. 2011;6:332-45.
7. Wang XD, Pang YJ, Ku G, Xie X, Stoica G, Wang LV. Noninvasive laser-induced photoacoustic tomography for structural and functional in vivo imaging of the brain. Nat Biotechnol. 2003;21:803-6.
8. Zhang HF, Maslov K, Stoica G, Wang L. Functional photoacoustic microscopy for high-resolution and noninvasive in vivo imaging. Nat Biotechnol. 2006;24:848-51.
9. Andreev VG, Karabutov AA, Oraevsky AA. Detection of ultrawide-band ultrasound pulses in optoacoustic tomography. IEEE Trans Ultrason Ferroelectr Freq Control. 2003;50:1383-90.
10. Eghtedari M, Copland JA, Kotov NA, Oraevsky AA, Motamedi M. Optoacoustic imaging of nanoparticle labeled breast cancer cells: a molecular based approach for imaging of deep tumors. Lasers Surg Med. 2004;S16:52.
11. Frangioni JV. New technologies for human cancer imaging. J Clin Oncol. 2008;26:4012-21.
12. Kruger RA, Lam RB, Reinecke DR, Del Rio SP, Doyle RP. Photoacoustic angiography of the breast. Med Phys. 2010;37:6096-100.
13. Kim C, Erpelding TN, Jankovic L, Pashley MD, Wang LV. Deeply penetrating in vivo photoacoustic imaging using a clinical ultrasound array system. Biomed Opt Express. 2010;1:278-84.
14. Pan DPJ, Cai X, Yalaz C, Senpan A, Omanakuttan K, Wickline SA, et al. Photoacoustic sentinel lymph node imaging with self-assembled copper neodecanoate nanoparticles. ACS Nano. 2012;6:1260-7.
15. Pan DPJ, Pramanik M, Senpan A, Ghosh S, Wickline SA, Wang LV, et al. Near infrared photoacoustic detection of sentinel lymph nodes with gold nanobeacons. Biomaterials. 2010;31:4088-93.
16. Song KH, Kim CH, Cobley CM, Xia Y, Wang LV. Near-infrared gold nanocages as a new class of tracers for photoacoustic sentinel lymph node mapping on a rat model. Nano Lett. 2009;9:183-8.
17. Song KH, Stein EW, Margenthaler JA, Wang LV. Noninvasive photoacoustic identification of sentinel lymph nodes containing methylene blue in vivo in a rat model. J Biomed Opt. 2008;13:054033.
18. Wang Y, Erpelding TN, Jankovic L, Guo Z, Robert JL, David G, et al. In vivo three-dimensional photoacoustic imaging based on a clinical matrix array ultrasound probe. J Biomed Opt. 2012;17:061208.
19. Staley J, Grogan P, Samadi AK, Cui H, Cohen MS, Yang X. Growth of melanoma brain tumors monitored by photoacoustic microscopy. J Biomed Opt. 2010;15:040510.
20. Kim C, Cho EC, Chen JY, Song KH, Au L, Favazza C, et al. In vivo molecular photoacoustic tomography of melanomas targeted by bioconjugated gold nanocages. ACS Nano. 2010;4:4559-64.
21. Galanzha EI, Shashkov EV, Spring PM, Suen JY, Zharov VP. In vivo, noninvasive, label-free detection and eradication of circulating metastatic melanoma cells using two-color photoacoustic flow cytometry with a diode laser. Cancer Res. 2009;69:7926-34.
22. Yao J, Maslov KI, Zhang Y, Xia Y, Wang LV. Label-free oxygen-metabolic photoacoustic microscopy in vivo. J Biomed Opt. 2011;16:076003.
23. Cheng Z, Levi J, Xiong ZM, Gheysens O, Keren S, Chen X. Near-infrared fluorescent deoxyglucose analogue for tumor optical imaging in cell culture and living mice. Bioconjugate Chem. 2006;17:662-9.
24. Qin CX, Cheng K, Chen K, Hu X, Liu Y, Lan X, et al. Tyrosinase as a multifunctional reporter gene for photoacoustic/MRI/PET triple modality molecular imaging. Sci Rep. 2013;3:1490.
25. Yang J-M, Chen R, Favazza C, Yao J, Zhou Q, Shung KK, et al. A 2.5-mm outer diameter photoacoustic endoscopic mini-probe based on a highly sensitive PMN-PT ultrasonic transducer. In: Oraevsky AA, Wang LV, eds. Photons Plus Ultrasound: Imaging and Sensing 2012. San Francisco, CA: SPIE; 2012: 82233M .
26. Wang B, Su JL, Karpiouk AB, Sokolov KV, Smalling RW, Emelianov SY. Intravascular photoacoustic imaging. IEEE J Quantum Electron. 2010;16:588-99.
27. Cobbold RSC. Foundations of Biomedical Ultrasound. Oxford: Oxford University Press; 2007.
28. Wang L. Photoacoustic Tomography—Ultrasonically Beating Optical Diffusion and Diffraction. San Francisco, CA: SPIE; 2014. http://spie.org/x106504.xml.
29. Azhari H. Basics of Biomedical Ultrasound for Engineers. Hoboken, NJ: Wiley-Interscience; 2010.
30. Moran CM, Bush NL, Bamber JC. Ultrasonic propagation properties of excised human skin. Ultrasound Med Biol. 1995;21:1177-90.

31. Kessler LW. VHF ultrasonic attenuation in mammalian tissue. J Acoust Soc Am. 1973;53:1759-60.
32. Maiti S, Shear JB, Williams RM, Zipfel WR, Webb WW. Measuring serotonin distribution in live cells with three-photon excitation. Science. 1997;275:530-2.
33. Diaspro A. Confocal and Two-Photon Microscopy: Foundations, Applications, and Advances. New York: Wiley-Liss; 2002.
34. Xu X, Liu H, Wang LV. Time-reversed ultrasonically encoded optical focusing into scattering media. Nat Photonics. 2011;5:154-7.
35. Wang YM, Judkewitz B, Dimarzio CA, Yang C. Deep-tissue focal fluorescence imaging with digitally time-reversed ultrasound-encoded light. Nat Commun. 2012;3:928.
36. Raju BI, Srinivasan MA. High-frequency ultrasonic attenuation and backscatter coefficients of in vivo normal human dermis and subcutaneous fat. Ultrasound Med Biol. 2001;27:1543-56.
37. Zackrisson S, van de Ven SM, Gambhir SS. Light in and sound out: emerging translational strategies for photoacoustic imaging. Cancer Res. 2014;74:979-1004.
38. Kim C, Favazza C, Wang LHV. In vivo photoacoustic tomography of chemicals: high-resolution functional and molecular optical imaging at new depths. Chem Rev. 2010;110:2756-82.
39. Ntziachristos V, Razansky D. Molecular imaging by means of multispectral optoacoustic tomography (MSOT). Chem Rev. 2010;110:2783-94.
40. Zhang HF, Maslov K, Li ML, Wang LV. In vivo volumetric imaging of subcutaneous microvasculature by photoacoustic microscopy. Opt Express. 2006;14:9317-23.
41. Zhou Y, Yi X, Xing W, Hu S, Maslov KI, Wang LV. Microcirculatory changes identified by photoacoustic microscopy in patients with complex regional pain syndrome type I after stellate ganglion blocks. J Biomed Opt. 2014;19:086017.
42. Song KH, Wang LV. Deep reflection-mode photoacoustic imaging of biological tissue. J Biomed Opt. 2007;12:060503.
43. Jeon M, Kim J, Kim C. Multiplane spectroscopic whole-body photoacoustic imaging of small animals in vivo. Med Biol Eng Comput. Published electronically August 12, 2014. doi:10.1007/s11517-014-1182-6
44. Maslov K, Zhang HF, Hu S, Wang LV. Optical-resolution photoacoustic microscopy for in vivo imaging of single capillaries. Opt Lett. 2008;33:929-31.
45. Zhang C, Maslov K, Wang LHV. Subwavelength-resolution label-free photoacoustic microscopy of optical absorption in vivo. Optics Lett. 2010;35:3195-7.
46. Cho Y, Chang CC, Yu J, Jeon M, Kim C, Wang LV, et al. Handheld photoacoustic tomography probe built using optical-fiber parallel acoustic delay lines. J Biomed Opt. 2014;19:086007.
47. Esenaliev RO, Karabutov AA, Oraevsky AA. Sensitivity of laser opto-acoustic imaging in detection of small deeply embedded tumors. IEEE J Sel Top Quant Electron. 1999;5:981-8.
48. Manohar S, Vaartjes SE, van Hespen JCG, Klaase JM, van den Engh FM, Steenbergen W, et al. Initial results of in vivo non-invasive cancer imaging in the human breast using near-infrared photoacoustics. Opt Express. 2007;15:12277-85.
49. Ermilov SA, Khamapirad T, Conjusteau A, Leonard MH, Lacewell R, Mehta K, et al. Laser optoacoustic imaging system for detection of breast cancer. J Biomed Opt. 2009;14:024007.
50. Kumon RE, Deng CX, Wang X. Frequency-domain analysis of photoacoustic imaging data from prostate adenocarcinoma tumors in a murine model. Ultrasound Med Biol. 2011;37:834-9.
51. Yaseen MA, Ermilov SA, Brecht HP, Su R, Conjusteau A, Fronheiser M, et al. Optoacoustic imaging of the prostate: development toward image-guided biopsy. J Biomed Opt. 2010;15:021310.
52. Silverman RH, Kong F, Chen YC, Lloyd HO, Kim HH, Cannata JM, et al. High-resolution photoacoustic imaging of ocular tissues. Ultrasound Med Biol. 2010;36:733-42.
53. Yang J-M, Favazza C, Chen RM, Yao J, Cai X, Maslov K, et al. Simultaneous functional photoacoustic and ultrasonic endoscopy of internal organs in vivo. Nat Med. 2012;18:1297-302.
54. Xia J, Chatni MR, Maslov K, Guo Z, Wang K, Anastasio M, et al. Whole-body ring-shaped confocal photoacoustic computed tomography of small animals in vivo. J Biomed Opt. 2012;17:050506.
55. Gateau J, Caballero MA, Dima A, Ntziachristos V. Three-dimensional optoacoustic tomography using a conventional ultrasound linear detector array: whole-body tomographic system for small animals. Med Phys. 2013;40:013302.

56. Brecht HP, Su R, Fronheiser M, Ermilov SA, Conjusteau A, Oraevsky AA. Whole-body three-dimensional optoacoustic tomography system for small animals. J Biomed Opt. 2009;14:064007.
57. Levi J, Kothapalli SR, Bohndiek S, Yoon JK, Dragulescu-Andrasi A, Nielsen C, et al. Molecular photoacoustic imaging of follicular thyroid carcinoma. Clin Cancer Res. 2013;19:1494-502.
58. Pramanik M, Ku G, Li C, Wang LV. Design and evaluation of a novel breast cancer detection system combining both thermoacoustic (TA) and photoacoustic (PA) tomography. Med Phys. 2008;35: 2218-23.
59. Strohm EM, Berndl ES, Kolios MC. High frequency label-free photoacoustic microscopy of single cells. Photoacoustics. 2013;1:49-53.
60. Strohm EM, Berndl ESL, Kolios MC. Probing red blood cell morphology using high-frequency photoacoustics. Biophys J. 2013;105:59-67.
61. Cai X, Li L, Krumholz A, Zhang C, Zhang Y, Xia Y, et al. Multi-scale molecular photoacoustic tomography of gene expression. PLoS ONE. 2012;7:e43999.
62. Hu S, Gonzales E, Soetikno B, Gong E, Yan P, Maslov K, et al. Optical-resolution photoacoustic microscopy of ischemic stroke. In: Oraevsky AA, Wang LV, eds. Photons Plus Ultrasound: Imaging and Sensing 2011. San Francisco, CA: SPIE; 2011: 789906.
63. Hu S, Maslov K, Tsytsarev V, Wang LV. Functional transcranial brain imaging by optical-resolution photoacoustic microscopy. J Biomed Opt. 2009;14:040503.
64. Hu S, Maslov K, Wang LV. Second-generation optical-resolution photoacoustic microscopy with improved sensitivity and speed. Optics Lett. 2011;36:1134-6.
65. Ku G, Maslov K, Li L, Wang LV. Photoacoustic microscopy with 2-mu m transverse resolution. J Biomed Opt. 2010;15:021302.
66. Liu YY, Yang XQ, Gong H, Jiang B, Wang H, Xu G, et al. Assessing the effects of norepinephrine on single cerebral microvessels using optical-resolution photoacoustic microscope. J Biomed Opt. 2013;18:076007.
67. Rao B, Maslov K, Danielli A, Chen R, Shung KK, Zhou Q, et al. Real-time four-dimensional optical-resolution photoacoustic microscopy with Au nanoparticle-assisted subdiffraction-limit resolution. Opt Lett. 2011;36:1137-9.
68. Tsytsarev V, Hu S, Yao JJ, Barbour DL, Wang LV. Photoacoustic microscopy of microvascular responses to cortical electrical stimulation. J Biomed Opt. 2011;16:076002.
69. Wang H, Yang XQ, Liu YY, Jiang B, Luo Q. Reflection-mode optical-resolution photoacoustic microscopy based on a reflective objective. Opt Express. 2013;21:24210-8.
70. Wang LD, Maslov K, Yao JJ, Rao B, Wang LV. Fast voice-coil scanning optical-resolution photoacoustic microscopy. Opt Lett. 2011;36:139-41.
71. Xia J, Li G, Wang LD, Nasiriavanaki M, Maslov K, Engelbach JA, et al. Wide-field two-dimensional multifocal optical-resolution photoacoustic-computed microscopy. Opt Lett. 2013;38:5236-9.
72. Xie ZX, Jiao SL, Zhang HF, Puliafito CA. Laser-scanning optical-resolution photoacoustic microscopy. Optics Lett. 2009;34:1771-3.
73. Xing WX, Wang LD, Maslov K, Wang LV. Integrated optical- and acoustic-resolution photoacoustic microscopy based on an optical fiber bundle. Optics Lett. 2013;38:52-4.
74. Yao JJ, Huang CH, Wang LD, Yang JM, Gao L, Maslov KI, et al. Wide-field fast-scanning photoacoustic microscopy based on a water-immersible MEMS scanning mirror. J Biomed Opt. 2012;17:080505.
75. Estrada H, Turner J, Kneipp M, Razansky D. Real-time optoacoustic brain microscopy with hybrid optical and acoustic resolution. Laser Phys Lett. 2014;11:045601.
76. Ma R, Sontges S, Shoham S, Ntziachristos V, Razansky D. Fast scanning coaxial optoacoustic microscopy. Biomed Opt Express. 2012;3:1724-31.
77. Li G, Maslov KI, Wang LV. Reflection-mode multifocal optical-resolution photoacoustic microscopy. J Biomed Opt. 2013;18:030501.
78. Song LA, Maslov K, Wang LV. Multifocal optical-resolution photoacoustic microscopy in vivo. Opt Lett. 2011;36:1236-8.
79. Langer G, Bouchal KD, Grun H, Burgholzer P, Berer T. Two-photon absorption-induced photoacoustic imaging of Rhodamine B dyed polyethylene spheres using a femtosecond laser. Opt Express. 2013;21:22410-22.

80. Yamaoka Y, Nambu M, Takamatsu T. Fine depth resolution of two-photon absorption-induced photoacoustic microscopy using low-frequency bandpass filtering. Opt Express. 2011;19:13365-77.
81. Urban BE, Yi J, Yakovlev V, Zhang HF. Investigating femtosecond-laser-induced two-photon photoacoustic generation. J Biomed Opt. 2014;19:085001.
82. Yao JJ, Wang LD, Li CY, Zhang C, Wang LV. Photoimprint photoacoustic microscopy for three-dimensional label-free subdiffraction imaging. Phys Rev Lett. 2014;112:014302.
83. Danielli A, Maslov K, Garcia-Uribe A, Winkler AM, Li C, Wang L, et al. Label-free photoacoustic nanoscopy. J Biomed Opt. 2014;19:086006.
84. Nedosekin DA, Galanzha EI, Dervishi E, Biris AS, Zharov VP. Super-resolution nonlinear photothermal microscopy. Small. 2014;10:135-42.
85. Deng ZL, Wang Z, Yang XQ, Luo Q, Gong H. In vivo imaging of hemodynamics and oxygen metabolism in acute focal cerebral ischemic rats with laser speckle imaging and functional photoacoustic microscopy. J Biomed Opt. 2012;17:081415.
86. Burton NC, Patel M, Morscher S, Driessen WH, Claussen J, Beziere N, et al. Multispectral opto-acoustic tomography (MSOT) of the brain and glioblastoma characterization. Neuroimage. 2013;65:522-8.
87. Liao LD, Lin CT, Shih YYI, Duong TQ, Lai HY, Wang PH, et al. Transcranial imaging of functional cerebral hemodynamic changes in single blood vessels using in vivo photoacoustic microscopy. J Cereb Blood Flow Metab. 2012;32:938-51.
88. Zhang HF, Maslov K, Sivaramakrishnan M, Stoica G, Wang LV. Imaging of hemoglobin oxygen saturation variations in single vessels in vivo using photoacoustic microscopy. Appl Phys Lett. 2007;90:053901.
89. Danielli A, Favazza CP, Maslov K, Wang LV. Single-wavelength functional photoacoustic microscopy in biological tissue. Opt Lett. 2011;36:769-71.
90. Guo ZJ, Hu S, Wang LHV. Calibration-free absolute quantification of optical absorption coefficients using acoustic spectra in 3D photoacoustic microscopy of biological tissue. Optics Lett. 2010;35: 2067-9.
91. Jo J, Yang X. Functional photoacoustic imaging to observe regional brain activation induced by cocaine hydrochloride. J Biomed Opt. 2011;16:090506.
92. Sivaramakrishnan M, Maslov K, Zhang HF, Stoica G, Wang LV. Limitations of quantitative photoacoustic measurements of blood oxygenation in small vessels. Phys Med Biol. 2007;52:1349-61.
93. Yang XM, Stein EW, Ashkenazi S, Wang LV. Nanoparticles for photoacoustic imaging. Wiley Interdiscip Rev Nanomed Nanobiotechnol. 2009;1:360-8.
94. Pramanik M, Wang LV. Thermoacoustic and photoacoustic sensing of temperature. J Biomed Opt. 2009;14:054024.
95. Winkler AM, Maslov K, Wang LV. Noise-equivalent sensitivity of photoacoustics. J Biomed Opt. 2013;18:097003.
96. Wang LD, Xia J, Yao JJ, Maslov KI, Wang LV. Ultrasonically encoded photoacoustic flowgraphy in biological tissue. Phys Rev Lett. 2013;111:204301.
97. Bauer AQ, Nothdurft RE, Erpelding TN, Wang LV, Culver JP. Quantitative photoacoustic imaging: correcting for heterogeneous light fluence distributions using diffuse optical tomography. J Biomed Opt. 2011;16:096016.
98. Brunker J, Beard P. Pulsed photoacoustic Doppler flowmetry using a cross correlation method. In: Oraevsky AA, Wang LV, eds. Photons Plus Ultrasound: Imaging and Sensing 2010. San Francisco, CA: SPIE; 2010: 756426.
99. Chen SL, Ling T, Huang SW, Baac HW, Guo LJ. Photoacoustic correlation spectroscopy and its application to low-speed flow measurement. Optics Lett. 2010;35:1200-2.
100. Fang H, Maslov K, Wang LV. Photoacoustic Doppler effect from flowing small light-absorbing particles. Phys Rev Lett. 2007;99:184501.
101. Sheinfeld A, Eyal A. Photoacoustic thermal diffusion flowmetry. Biomed Opt Express. 2012;3:800-13.
102. Wang L, Yao J, Maslov KI, Xing W, Wang LV. Ultrasound-heated photoacoustic flowmetry. J Biomed Opt. 2013;18:117003

103. Yao JJ, Wang LHV. Transverse flow imaging based on photoacoustic Doppler bandwidth broadening. J Biomed Opt. 2010;15:021304.
104. Chatni MR, Yao JJ, Danielli A, Favazza CP, Maslov KI, Wang LV. Functional photoacoustic microscopy of pH. J Biomed Opt. 2011;16:100503.
105. Duan ZY, Gao YJ, Qiao ZY, Fan G, Liu Y, Zhang D, et al. A photoacoustic approach for monitoring the drug release of pH-sensitive poly(beta-amino ester)s. J Mater Chem B. 2014;2:6271-82.
106. Huang GJ, Si Z, Yang SH, Li C, Xing D. Dextran based pH-sensitive near-infrared nanoprobe for in vivo differential-absorption dual-wavelength photoacoustic imaging of tumors. J Mater Chem. 2012;22:22575-81.
107. Horvath TD, Kim G, Kopelman R, Ashkenazi S. Ratiometric photoacoustic sensing of pH using a "sonophore." Analyst. 2008;133:747-9.
108. MacKenzie HA, Ashton HS, Spiers S, Shen Y, Freeborn SS, Hannigan J, et al. Advances in photoacoustic noninvasive glucose testing. Clin Chem. 1999;45:1587-95.
109. Yeh C, Hu S, Maslov K, Wang LV. Photoacoustic microscopy of blood pulse wave. J Biomed Opt. 2012;17:070504.
110. Song W, Wei Q, Liu WZ, Yi J, Sheibani N, Fawzi AA, et al. A combined method to quantify the retinal metabolic rate of oxygen using photoacoustic ophthalmoscopy and optical coherence tomography. Sci Rep. 2014;4:6525.
111. Liu T, Wei Q, Wang J, Jiao S, Zhang HF. Combined photoacoustic microscopy and optical coherence tomography can measure metabolic rate of oxygen. Biomed Opt Express. 2011;2:1359-65.
112. Hsia CC. Respiratory function of hemoglobin. N Engl J Med. 1998;338:239-47.
113. Dean-Ben XL, Bay E, Razansky D. Functional optoacoustic imaging of moving objects using microsecond-delay acquisition of multispectral three-dimensional tomographic data. Sci Rep. 2014;4:5878.
114. Cox B, Laufer JG, Arridge SR, Beard PC. Quantitative spectroscopic photoacoustic imaging: a review. J Biomed Opt. 2012;17:061202.
115. Luis Dean-Ben X, Razansky D. Adding fifth dimension to optoacoustic imaging: volumetric time-resolved spectrally enriched tomography. Light Sci Appl. 2014;3:e137.
116. Maslov K, Zhang HF, Wang LV. Effects of wavelength-dependent fluence attenuation on the noninvasive photoacoustic imaging of hemoglobin oxygen saturation in subcutaneous vasculature in vivo. Inverse Probl. 2007;23:S113-22.
117. Wang J, Liu T, Jiao SL, Chen R, Zhou Q, Shung KK, et al. Saturation effect in functional photoacoustic imaging. J Biomed Opt. 2010;15:021317.
118. Xie ZX, Wang LHV, Zhang HF. Optical fluence distribution study in tissue in dark-field confocal photoacoustic microscopy using a modified Monte Carlo convolution method. Appl Opt. 2009;48:3204-11.
119. Xia J, Danielli A, Liu Y, Wang L, Maslov K, Wang LV. Calibration-free quantification of absolute oxygen saturation based on the dynamics of photoacoustic signals. Opt Lett. 2013;38:2800-3.
120. Shao Q, Morgounova E, Jiang C, Choi J, Bischof J, Ashkenazi S. In vivo photoacoustic lifetime imaging of tumor hypoxia in small animals. J Biomed Opt. 2013;18:076019.
121. Mallidi S, Luke GP, Emelianov S. Photoacoustic imaging in cancer detection, diagnosis, and treatment guidance. Trends Biotechnol. 2011;29:213-21.
122. Schule G, Huttmann G, Framme C, Roider J, Brinkmann R. Noninvasive optoacoustic temperature determination at the fundus of the eye during laser irradiation. J Biomed Opt. 2004;9:173-9.
123. Larina IV, Larin KV, Esenaliev RO. Real-time optoacoustic monitoring of temperature in tissues. J Phys D Appl Phys. 2005;38:2633-9.
124. Kandulla J, Elsner H, Birngruber R, Brinkmann R. Noninvasive optoacoustic online retinal temperature determination during continuous-wave laser irradiation. J Biomed Opt. 2006;11:041111.
125. Nikitin SM, Khokhlova TD, Pelivanov IM. Temperature dependence of the optoacoustic transformation efficiency in ex vivo tissues for application in monitoring thermal therapies. J Biomed Opt. 2012;17:061214.
126. Petrova EV, Ermilov S, Su R, Nadvoretskiy V, Conjusteau A, Oraevsky A. Using optoacoustic imaging for measuring the temperature dependence of Gruneisen parameter in optically absorbing solutions. Opt Express. 2013;21:25077-90.

127. Petrova EV, Oraevsky AA, Ermilov SA. Red blood cell as a universal optoacoustic sensor for non-invasive temperature monitoring. Appl Phys Lett. 2014;105:094103.
128. Serebryakov VA, Boiko EV, Yan AV. Real-time optoacoustic monitoring of the temperature of the retina during laser therapy. J Opt Technol. 2014;81:312-21.
129. Rao KS, Yehya F, Chaudhary AK, Kumar AS, Sahoo AK. Thermal stability study of nitro-rich triazole derivatives using temperature dependent time resolved pulsed photoacoustic (PA) technique. J Anal Appl Pyrol. 2014;109:132-9.
130. Shah J, Park S, Aglyamov S, Larson T, Ma L, Sokolov K, et al. Photoacoustic imaging and temperature measurement for photothermal cancer therapy. J Biomed Opt. 2008;13:034024.
131. Yao J, Wang LV. Photoacoustic microscopy. Laser Photonics Rev. 2013;7:758-78.
132. Yao L, Huang H, Jiang H. Finite-element-based photoacoustic imaging of absolute temperature in tissue. Opt Lett. 2014;39:5355-8.
133. Zhang R, Wang L, Yao J, Yeh C-H, Wang LV. In vivo optically encoded photoacoustic flowgraphy. Opt Lett. 2014;39:3814-7.
134. Fang H, Maslov K, Wang LV. Photoacoustic Doppler flow measurement in optically scattering media. Appl Phys Lett. 2007;91:264103.
135. Sheinfeld A, Gilead S, Eyal A. Time-resolved photoacoustic Doppler characterization of flow using pulsed excitation. In: Oraevsky AA, Wang LV, eds. Photons Plus Ultrasound: Imaging and Sensing 2010. San Francisco, CA: SPIE; 2010: 75643N.
136. Yao J, Maslov KI, Shi Y, Taber LA, Wang LV. In vivo photoacoustic imaging of transverse blood flow by using Doppler broadening of bandwidth. Optics Lett. 2010;35:1419-221.
137. Yao JJ, Gilson RC, Maslov KI, Wang L, Wang LV. Calibration-free structured-illumination photoacoustic flowgraphy of transverse flow in scattering media. J Biomed Opt. 2014;19:046007.
138. Zhang RY, Yao JJ, Maslov KI, Wang LV. Structured-illumination photoacoustic Doppler flowmetry of axial flow in homogeneous scattering media. Appl Phys Lett. 2013;103:094101.
139. Razansky D, Buehler A, Ntziachristos V. Volumetric real-time multispectral optoacoustic tomography of biomarkers. Nat Protoc. 2011;6:1121-9.
140. Razansky D, Distel M, Vinegoni C, Ma R, Perrimon N, Köster RW, et al. Multispectral optoacoustic tomography of deep-seated fluorescent proteins in vivo. Nat Photonics. 2009;3:412-7.
141. Razansky D, Vinegoni C, Ntziachristos V. Multispectral photoacoustic imaging of fluorochromes in small animals. Opt Lett. 2007;32:2891-3.
142. de la Zerda A, Kim JW, Galanzha EI, Gambhir SS, Zharov VP. Advanced contrast nanoagents for photoacoustic molecular imaging, cytometry, blood test and photothermal theranostics. Contrast Media Mol I. 2011;6:346-69.
143. Galanzha EI, Shashkov EV, Kelly T, Kim J-W, Yang L, Zharov VP. In vivo magnetic enrichment and multiplex photoacoustic detection of circulating tumour cells. Nature Nanotechnology 2009;4:855-60.
144. Taruttis A, Herzog E, Razansky D, Ntziachristos V. Real-time imaging of cardiovascular dynamics and circulating gold nanorods with multispectral optoacoustic tomography. Opt Express. 2010;18:19592-602.
145. Wang YW, Xie XY, Wang XD, Ku G, Gill KL, O'Neal DP, et al. Photoacoustic tomography of a nanoshell contrast agent in the in vivo rat brain. Nano Lett. 2004;4:1689-92.
146. Su R, Ermilov SA, Liopo AV, Oraevsky AA. Three-dimensional optoacoustic imaging as a new noninvasive technique to study long-term biodistribution of optical contrast agents in small animal models. J Biomed Opt. 2012;17:101506.
147. Juratli MA, Sarimollaoglu M, Siegel ER, Nedosekin DA, Galanzha EI, Suen JY, et al. Real-time monitoring of circulating tumor cell release during tumor manipulation using in vivo photoacoustic and fluorescent flow cytometry. Head Neck. 2014;36:1207-15.
148. Kircher MF, de la Zerda A, Jokerst JV, Zavaleta CL, Kempen PJ, Mittra E, et al. A brain tumor molecular imaging strategy using a new triple-modality MRI-photoacoustic-Raman nanoparticle. Nat Med. 2012;18:829-34.
149. Laufer J, Jathoul A, Johnson P, Zhang E, Lythgoe M, Pedley RB, et al. In vivo photoacoustic imaging of tyrosinase expressing tumours in mice. In: Oraevsky AA, Wang LV, eds. Photons Plus Ultrasound: Imaging and Sensing 2012. San Francisco, CA: SPIE; 2012: 82230M .

150. Tsyboulski DA, Liopo AV, Su R, Ermilov SA, Bachilo SM, Weisman RB, et al. Enabling in vivo measurements of nanoparticle concentrations with three-dimensional optoacoustic tomography. J Biophotonics. 2014;7:581-8.
151. Yao J, Wang LV. Sensitivity of photoacoustic microscopy. Photoacoustics. 2014;2:87-101.
152. Bouchard LS, Anwar MS, Liu GL, Hann B, Xie ZH, Gray JW, et al. Picomolar sensitivity MRI and photoacoustic imaging of cobalt nanoparticles. Proc Natl Acad Sci U S A. 2009;106:4085-9.
153. de la Zerda A, Liu ZA, Bodapati S, Teed R, Vaithilingam S, Khuri-Yakub BT, et al. Ultrahigh sensitivity carbon nanotube agents for photoacoustic molecular imaging in living mice. Nano Lett. 2010;10:2168-72.
154. Oraevsky AA, Karabutov AA. Ultimate sensitivity of time-resolved optoacoustic detection. In: Oraevsky AA, ed. Biomedical Optoacoustics. San Jose, CA: SPIE; 2000: 228-239.
155. Razansky D, Baeten J, Ntziachristos V. Sensitivity of molecular target detection by multispectral optoacoustic tomography (MSOT). Med Phys. 2009;36:939-45.
156. Eghtedari M, Oraevsky A, Copland JA, Kotov NA, Conjusteau A, Motamedi M. High sensitivity of in vivo detection of gold nanorods using a laser optoacoustic imaging system. Nano Lett. 2007;7:1914-8.
157. Copland JA, Eghtedari M, Popov VL, Kotov N, Mamedova N, Motamedi M. Bioconjugated gold nanoparticles as a molecular based contrast agent: implications for imaging of deep tumors using optoacoustic tomography. Mol Imaging Biol. 2004;6:341-9.
158. Chatni MR, Xia J, Sohn R, Maslov K, Guo Z, Zhang Y, et al. Tumor glucose metabolism imaged in vivo in small animals with whole-body photoacoustic computed tomography. J Biomed Opt. 2012;17:076012.
159. Yao J, Xia J, Maslov KI, Nasiriavanaki M, Tsytsarev V, Demchenko AV. Noninvasive photoacoustic computed tomography of mouse brain metabolism in vivo. Neuroimage. 2013;64:257-66.
160. Galanzha EI, Nedosekin DA, Sarimollaoglu M, Orza AI, Biris AS, Verkhusha VV, et al. Photoacoustic and photothermal cytometry using photoswitchable proteins and nanoparticles with ultrasharp resonances. J Biophotonics. 2015;8:81-93.
161. Wang Y, Maslov K, Zhang Y, Hu S, Yang L, Xia Y, et al. Fiber-laser-based photoacoustic microscopy and melanoma cell detection. J Biomed Opt. 2011;16:011014.
162. Bhattacharyya K, Goldschmidt BS, Hannink M, Alexander S, Viator JA. Gold nanoparticle-mediated detection of circulating cancer cells. Clin Lab Med. 2012;32:89-101.
163. Tzoumas S, Nunes A, Deliolanis NC, Ntziachristos V. Effects of multispectral excitation on the sensitivity of molecular optoacoustic imaging. J Biophotonics. 2014;9999:9999.
164. Wang Y, Maslov K, Wang LHV. Spectrally encoded photoacoustic microscopy using a digital mirror device. J Biomed Opt. 2012;17:066020.
165. Wang L, Maslov K, Wang LV. Single-cell label-free photoacoustic flowoxigraphy in vivo. Proc Natl Acad Sci U S A. 2013;110:5759-64.
166. Li XQ, Xi L, Jiang RX, Yao L, Jiang H. Integrated diffuse optical tomography and photoacoustic tomography: phantom validations. Biomed Opt Express. 2011;2:2348-53.
167. Xiaoqi L, Huabei J. Impact of inhomogeneous optical scattering coefficient distribution on recovery of optical absorption coefficient maps using tomographic photoacoustic data. Phys Med Biol. 2013;58:999-1011.
168. Xu C, Kumavor PD, Alqasemi U, Li H, Xu Y, Zanganeh S, et al. Indocyanine green enhanced co-registered diffuse optical tomography and photoacoustic tomography. J Biomed Opt. 2013;18:126006.
169. Yin L, Wang Q, Zhang Q, Jiang H. Tomographic imaging of absolute optical absorption coefficient in turbid media using combined photoacoustic and diffusing light measurements. Opt Lett. 2007;32:2556-8.
170. Xia J, Huang C, Maslov K, Anastasio MA, Wang LV. Enhancement of photoacoustic tomography by ultrasonic computed tomography based on optical excitation of elements of a full-ring transducer array. Opt Lett. 2013;38:3140-3.
171. Treeby BE. Acoustic attenuation compensation in photoacoustic tomography using time-variant filtering. J Biomed Opt. 2013;18:036008.

172. Dean-Ben XL, Razansky D, Ntziachristos V. The effects of acoustic attenuation in optoacoustic signals. Phys Med Biol. 2011;56:6129-48.
173. Dean-Ben XL, Ntziachristos V, Razansky D. Artefact reduction in optoacoustic tomographic imaging by estimating the distribution of acoustic scatterers. J Biomed Opt. 2012;17:110504.
174. Li L, Maslov K, Ku G, Wang LV. Three-dimensional combined photoacoustic and optical coherence microscopy for in vivo microcirculation studies. Opt Express. 2009;17:16450-5.
175. Akers WJ, Edwards WB, Kim C, Xu B, Erpelding TN, Wang LV, et al. Multimodal sentinel lymph node mapping with single-photon emission computed tomography (SPECT)/computed tomography (CT) and photoacoustic tomography. Transl Res. 2012;159:175-81.
176. Wang Y, Hu S, Maslov K, Zhang Y, Xia Y, Wang LV. In vivo integrated photoacoustic and confocal microscopy of hemoglobin oxygen saturation and oxygen partial pressure. Opt Lett. 2011;36:1029-31.
177. Abran M, Cloutier G, Cardinal MH, Chayer B, Tardif JC, Lesage F. Development of a photoacoustic, ultrasound and fluorescence imaging catheter for the study of atherosclerotic plaque. IEEE Trans Biomed Circuits Syst. 2014;8:696-703.
178. Jiao SL, Jiang MS, Hu JM, Fawzi A, Zhou Q, Shung KK, et al. Photoacoustic ophthalmoscopy for in vivo retinal imaging. Opt Express. 2010;18:3967-72.
179. Song W, Wei Q, Liu T, Kuai D, Burke JM, Jiao S, et al. Integrating photoacoustic ophthalmoscopy with scanning laser ophthalmoscopy, optical coherence tomography, and fluoresce in angiography for a multimodal retinal imaging platform. J Biomed Opt. 2012;17:061206-7.
180. Tsytsarev V, Rao B, Maslov KI, Li L, Wang L. Photoacoustic and optical coherence tomography of epilepsy with high temporal and spatial resolution and dual optical contrasts. J Neurosci Meth. 2013;216:142-5.
181. Lee C, Han S, Kim S, Jeon M, Jeon MY, Kim C, et al. Combined photoacoustic and optical coherence tomography using a single near-infrared supercontinuum laser source. Appl Opt. 2013;52:1824-8.
182. Wilson KE, Wang TY, Willmann JK. Acoustic and photoacoustic molecular imaging of cancer. J Nucl Med. 2013;54:1851-4.
183. Harrison T, Ranasinghesagara JC, Lu HH, Mathewson K, Walsh A, Zemp RJ. Combined photoacoustic and ultrasound biomicroscopy. Opt Express. 2009;17:22041-6.
184. Rao B, Soto F, Kerschensteiner D, Wang LV. Integrated photoacoustic, confocal, and two-photon microscope. J Biomed Opt. 2014;19:36002.
185. Lai P, Wang L, Tay JW, Wang LV. Nonlinear photoacoustic wavefront shaping (PAWS) for single speckle-grain optical focusing in scattering media. Nat Photonics. 2015; 9: 126-132.
186. Conkey DB, Caravaca-Aguirre AM, Dove JD, Ju H, Murray TW, Piestun R. Super-resolution photoacoustic imaging through a scattering wall. arXiv. 2013;1310.5736. Available from url: arxiv.org/abs/1310.5736.
187. Li H, Dong BQ, Zhang Z, Zhang HF, Sun C. A transparent broadband ultrasonic detector based on an optical micro-ring resonator for photoacoustic microscopy. Sci Rep. 2014;4:4496.
188. Zhang EZ, Beard PC. A miniature all-optical photoacoustic imaging probe. In: Oraevsky AA, Wang LV, eds. Photons Plus Ultrasound: Imaging and Sensing 2011. San Francisco, CA: SPIE; 2011: 78991F.
189. Chen SL, Xie ZX, Ling T, Guo LJ, Wei X, Wang X. Miniaturized all-optical photoacoustic microscopy based on microelectromechanical systems mirror scanning. Opt Lett. 2012;37:4263-5.
190. Miida Y, Matsuura Y. Optical-fiber based all-optical 3D photoacoustic imaging system. In: Oraevsky AA, Wang LV, eds. Photons Plus Ultrasound: Imaging and Sensing 2014. San Francisco, CA: SPIE; 2014: 894331.
191. Bell MAL, Guo X, Song DY, Boctor EM. Photoacoustic imaging of prostate brachytherapy seeds with transurethral light delivery. In: Oraevsky AA, Wang LV, eds. Photons Plus Ultrasound: Imaging and Sensing 2014. San Francisco, CA: SPIE; 2014: 89430N.
192. Viator JA, Au G, Paltauf G, Jacques SL, Prahl SA, Ren H. Clinical testing of a photoacoustic probe for port wine stain depth determination. Laser Surg Med. 2002;30:141-8.

193. Yuan KH, Yuan Y, Gu Y, Gao J, Xing D. In vivo photoacoustic imaging of model of port wine stains. J Xray Sci Technol. 2012;20:249-54.
194. Brecht HP, Prough DS, Petrov YY, Patrikeev I, Petrova IY, Deyo DJ, et al. In vivo monitoring of blood oxygenation in large veins with a triple-wavelength optoacoustic system. Opt Express. 2007;15: 16261-9.
195. Kim C, Erpelding TN, Maslov K, Jankovic L, Akers WJ, Song L, et al. Handheld array-based photoacoustic probe for guiding needle biopsy of sentinel lymph nodes. J Biomed Opt. 2010;15:046010.
196. Dean-Ben XL, Razansky D. Functional optoacoustic human angiography with handheld video rate three dimensional scanner. Photoacoustics. 2013;1:68-73.
197. Zhou Y, Xing WX, Maslov KI, Cornelius LA, Wang LV. Handheld photoacoustic microscopy to detect melanoma depth in vivo. Opt Lett. 2014;39:4731-4.
198. Adachi Y, Hoshimiya T. Photoacoustic imaging with multiple-wavelength light-emitting diodes. Jpn J Appl Phys. 2013;52:07HB06.
199. Bell MAL, Guo X, Kang HJ, Boctor E. Improved contrast in laser-diode-based photoacoustic images with short-lag spatial coherence beamforming. In: Ultrasonics Symposium (IUS), 2014 IEEE International. Chicago, IL: IEEE; 2014. pp. 37-40.
200. Zeng LM, Liu GD, Yang DW, Ji X. 3D-visual laser-diode-based photoacoustic imaging. Opt Express. 2012;20:1237-46.
201. Kolkman RGM, Steenbergen W, van Leeuwen TG. In vivo photoacoustic imaging of blood vessels with a pulsed laser diode. Laser Med Sci. 2006;21:134-9.
202. Li M-L, Wang P-H. Optical resolution photoacoustic microscopy using a Blu-ray DVD pickup head. In: Oraevsky AA, Wang LV, eds. Photons Plus Ultrasound: Imaging and Sensing 2014. San Francisco, CA: SPIE; 2014: 894315.
203. Yapici MK, Kim C, Chang CC, Jeon M, Guo Z, Cai X, et al. Parallel acoustic delay lines for photoacoustic tomography. J Biomed Opt. 2012;17:116019.
204. Pu KY, Shuhendler AJ, Jokerst JV, Mei J, Gambhir SS, Bao Z, et al. Semiconducting polymer nanoparticles as photoacoustic molecular imaging probes in living mice. Nat Nanotechnol. 2014;9:233-9.